Catalysis Today 146 (2009) 160–165

Contents lists available at ScienceDirect

Catalysis Today

journal homepage: www.elsevier.com/locate/cattod

Pt–Co bimetallic catalyst supported on single walled carbon nanotube: XAS and aqueous phase reforming activity studies

Xiaoming Wang, Nan Li, Lisa D. Pfefferle, Gary L. Haller *

Department of Chemical Engineering, Yale University P.O. Box 208286, New Haven, CT 06520-8286, USA

ARTICLE INFO

Keywords:
Aqueous phase reforming
Bimetallic catalyst
Carbon nanotube
Hydrogen generation
Biofuel
Fuel cell

ABSTRACT

We have developed a simple method to create a catalyst with atomically dispersed Pt on top of Co nanoparticles on single walled carbon nanotubes (SWNT) supports by sequential impregnation of Pt(II) and Co(II) solutions following by hydrogen reduction. The aqueous phase reforming activity is much higher than for Pt monometallic catalysts on SWNT supports prepared by several methods, either pre-reduced in hydrogen or in the liquid phase. The high selectivity of the monometallic catalysts is maintained for the bimetallic systems. The Extended X-ray Absorption Fine Structure (EXAFS) results at the Pt L_{III} edge show no observable Pt–Pt bond. Only Pt–Co bonds were observed, indicating high dispersion of Pt. The enhanced activity comes from two sources: the high dispersion of Pt and the effect of the Co as co-catalyst or modifier. This contribution demonstrates the possibility to further engineer bimetallic catalysts to improve the aqueous phase reforming activity, especially to retain good selectivity at high conversion.

1. Introduction

Hydrogen fuel cells are promising devices for clean and efficient energy for a variety of applications [1]. The current hydrogen production method, the steam reforming of hydrocarbons from fossil fuels, however, is not environmentally friendly. In addition, the carbon monoxide (CO) impurity in the hydrogen stream from the steam reforming products causes poisoning of the fuel cell anode catalyst [2].

Dumesic and co-workers have developed an aqueous phase reforming (APR) process which uses an oxide (alumina or silica) supported Pt catalyst to catalyze the reforming of oxygenated hydrocarbons in aqueous solution at relatively low temperature (200–250 °C), to produce hydrogen and carbon dioxide (CO_2) with a low level of CO [3]. The reaction can be stoichiometrically written as (taking ethylene glycol for example):

$$C_2H_6O_2 + 2H_2O \rightarrow 5H_2 + 2CO_2$$

However, the oxide supports are not very stable in the aqueous phase at these reaction conditions. Therefore, less reactive or inert catalyst supports are desired for APR. Recently we have decorated Pt nanoparticles on single walled carbon nanotubes (SWNT) using a wet-reduction method, and this Pt–SWNT catalyst showed higher APR activity than the alumina supported catalyst. In addition, the catalytic activity and selectivity remained unchanged after a week of steady-state reaction. We also developed a Pt–Co bimetallic catalyst supported on SWNT by separately decorating Pt and Co nanoparticles on SWNT. This Pt–Co on SWNT catalyst increased the APR activity five fold compared with the Pt–SWNT catalyst from the wet-reduction method. The Extended X-ray Absorption Fine Structure (EXAFS) results indicated the co-existence of Pt and Co nanoparticles with no Pt–Co bimetallic phase [4].

Huber et al. also showed that adding Co to a Pt/alumina catalyst significantly increased the activity of the catalyst [5]. They used an incipient wetness impregnation method for both Pt and Co, thus their catalyst is more likely to have bimetallic Pt–Co nano-alloy particles than individual Pt and Co nanoparticles, but no detailed research has been carried out to understand the structure of the metal species on the sequentially impregnated Pt–Co bimetallic APR catalyst.

In this work, we prepared the Pt–Co/SWNT catalyst using an incipient wetness impregnation method and tested its APR activity. Shabaker et al. have compared a variety of supports for Pt APR [6] that included activated carbon, which had comparable activity to an alumina support. Different temperature and pressure of reaction prohibit a direct comparison with the SWNT activity reported in this work. APR reaction was also performed on Pt/SWNT catalyst prepared by a similar incipient wetness impregnation method and Pt–SWNT catalyst prepared by a wet-reduction

* Corresponding author. Tel.: +1 230 432 4378; fax: +1 203 432 4387.
E-mail address: gary.haller@yale.edu (G.L. Haller).

0920-5861/$ – see front matter © 2009 Published by Elsevier B.V.
doi:10.1016/j.cattod.2009.02.010

method for comparison. In-situ X-ray absorption spectroscopy (XAS) was utilized to obtain the structure and oxidation state information on the catalysts and to explore the structure–activity relationship.

The Pt–Co bimetallic system can stoichiometrically form PtCo, $PtCo_3$, and Pt_3Co alloy phases, with both crystalline (ordered) and amorphous (disordered) structures [7], and at mild temperatures as used in this work, it is likely to form an amorphous random alloy [8]. A detailed X-ray Absorption Near Edge Structure (XANES) study also indicated that the formation of a Pt–Co alloy phase would cause electron transfer between these two elements, which leads to the change of white line intensity and other near edge characteristic peaks [9]. However, these previous experiments were all performed on bulk phase Pt–Co alloys, not extending to nano-alloys. Recently Pt–Co bimetallic nanoparticles have been developed for catalysis [10,11], electrochemistry [12,13] and supermagnetic recording materials [14,15]. XAS analysis has been done [10,11] on Pt–Co bimetallic catalysts impregnated on alumina or zeolite supports with Pt as the minor component of the bimetallic system. However, they all conclude that from XAS, they can observe Pt–Co bonding at the Pt L_{III} edge, but cannot see Co–Pt bonding at the Co K edge, which is not consistent with mass conservation. In this paper we would like to present a detailed XAS spectral analysis to further explore the Pt–Co bimetallic structure in a nano-alloyed particle supported on carbon nanotubes.

2. Experimental

2.1. Catalyst synthesis

The SWNT used in this research was purchased from Cheap Tubes Inc., and labeled as cSWNT. The surface area of the cSWNT is 407 m^2/g and the pore volume is 2 cm^3/g. The carbon nanotubes were refluxed with 2.6 M nitric acid overnight, filtered and dried for further use.

The Pt on SWNT catalyst was prepared by incipient wetness impregnation. Tetra-ammine platinum(II) nitrate (from Strem Chemicals) was dissolved in water and the solution was added to the nitric acid treated SWNT dropwise until incipient wetness. The catalyst was labeled as Pt/cSWNT, and the loading of Pt was 8.0 wt%, which is confirmed by the edge jump of X-ray absorption [16]. The Pt–Co bimetallic catalyst was prepared by a sequential impregnation method. Pt/cSWNT was prepared as stated above and dried at 60 °C over night, and then cobalt(II) nitrate (from Sigma–Aldrich) solution was added to the already-prepared Pt/cSWNT dropwise until incipient wetness. Equal weights of Pt and Co were used, thus the molar ratio of Pt to Co is 0.30. Both Pt/cSWNT and Pt–Co/cSWNT were air dried at 150 °C before use.

The wet-reduction method has been described elsewhere [17] and applied to our lab-made SWNT [4] before. Potassium tetrachloroplatinate(II) (from Sigma–Aldrich) was dissolved in ethylene glycol–water mixture with nitric acid treated cSWNT and refluxed for 8 h. The product was filtered, dried and labeled Pt–cSWNT–EG.

2.2. Activity test

The APR activity test was carried out in a fixed bed reactor followed by a condenser and a gas–liquid separator, and the design is reported elsewhere [5]. Fifty milligrams of catalyst was placed in the reactor and 10 wt% ethylene glycol aqueous solution was introduced into the reactor at 60 μL/min via an HPLC pump. The reaction was carried out at 225 °C and 380 psig, and the gas products were analyzed by an online Varian CP-3800 gas chromatography.

2.3. Structural analysis

X-ray absorption experiments were carried out at beamline X18B at NSLS, Brookhaven National Lab. Around 30 mg of the catalyst was well mixed with 270 mg boron nitride power by grinding, and then pressed into a self supporting pellet which was then placed in a stainless steel in-situ reaction cell. Data were collected at both the Co K edge (7709 eV) and the Pt L_{III} edge (11564 eV) in transmission mode, and a corresponding metal foil was used as an internal reference. The catalysts were reduced in-situ in flowing hydrogen, and the temperature was first ramped up to 400 °C in 20 min, and then held for 30 min. Time-resolved XANES spectra were measured throughout this procedure. After reduction, the system was cooled to room temperature in flowing hydrogen by liquid nitrogen. Extended X-ray absorption fine structure was measured before and after reduction, both at room temperature. The EXAFS data was analyzed and fitted using the IFEFFIT 1.2.10 software package [18].

3. Results and discussion

3.1. APR activity results

The catalyst activity and selectivity data for both monometallic and bimetallic catalyst systems supported on cSWNT supports are shown in Table 1. Among the monometallic catalysts, the Pt–cSWNT–EG catalyst prepared from the wet-reduction method shows higher activity than the Pt/cSWNT catalyst prepared from the incipient wetness impregnation method, with the latter showing almost no hydrogen production. However, the Pt–Co/cSWNT catalyst prepared from the sequential impregnation method shows 3 times higher activity than the Pt–cSWNT–EG catalyst, while the selectivity is not much affected. Some of the reactivity data from the literature are also compared here, from

Table 1
The aqueous phase reforming reactivity of different Pt and Pt–Co catalyst supported on different SWNT supports.

Catalyst	Pre-reduction	Catalyst mass time yield[a]	Pt mass time yield[b]	Conversion[c]	Hydrogen selectivity[d]	Alkane selectivity[e]
Pt–cSWNT–EG	No	0.51	6.5	4.5%	92%	12.6%
Pt/cSWNT	Yes	N/A[f]	N/A[f]	0.4%	N/A[f]	11.7%
Pt–Co/cSWNT	Yes	1.78	24.7	16.5%	~100%	7.1%
Pt/Al_2O_3[g]	Yes	0.45	15	5.4%	87%	1.2%
$Pt–Co/Al_2O_3$[g]	Yes	0.69	23	8.4%	88%	0.5%

[a] Measured by millimole hydrogen per gram catalyst per minute.
[b] Measured by millimole hydrogen per gram platinum in the catalyst per minute.
[c] Evaluated by CO_2 production with respect to the ethylene glycol feed.
[d] Calculated as (molecules H_2 produced/C atoms in gas phase)(2/5).
[e] Calculated as (C atoms in gaseous alkanes)/(total C atoms in gas-phase product).
[f] The hydrogen yield for this catalyst is below the detection limit.
[g] Reference data from Huber et al. [5].

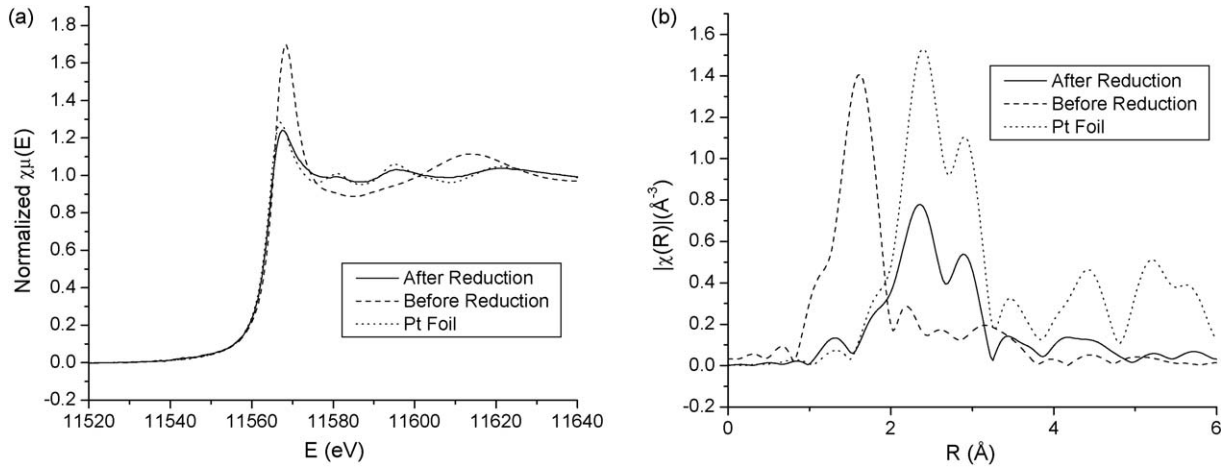

Fig. 1. XAS results of Pt/cSWNT before and after reduction. (a) XANES spectra; (b) R space of the EXAFS spectra.

which one can conclude that SWNT supported catalysts have better hydrogen selectivity, but somewhat poorer alkane selectivity compared with alumina supported catalysts.

3.2. Pt monometallic catalyst

The structural study of the catalyst prepared by the wet-reduction method has already been reported in our previous paper [4]. The catalyst prepared by this method was shown to contain Pt(0) nanoparticles with 2–3 nm in diameter. This catalyst, thus, does not require pre-reduction before use for the APR reaction. However, for the Pt/cSWNT catalyst prepared by incipient wetness impregnation, pre-reduction is desired. Therefore, in order to investigate the structure of the catalyst, XAS was utilized to study the reduction process of Pt/cSWNT.

Fig. 1(a) shows the XANES spectra of Pt/cSWNT before and after in-situ hydrogen reduction, and the results of Pt foil is also shown for comparison. From Fig. 1 we can see that after reduction, the Pt species has been reduced to Pt(0). It should be noted that the XANES spectrum of the reduced Pt/cSWNT and that of the Pt foil are not identical, which is probably caused by the chemisorbed hydrogen, as has been reported previously for Pt catalyst in a hydrogen atmosphere with other support systems [19,20]. Another possible reason for the XANES difference between the Pt/cSWNT catalyst and Pt foil is from the interaction of Pt with the SWNT support, which has been suggested by Zhou et al. [21]. However, in the work of Zhou et al., a multiwalled carbon nanotube support was used which, while exposed to air, was not highly oxidized and the interaction was assumed to be directly with carbon defects. In our case, the support in SWNT that has been oxidized by nitric acid and the interaction is presumed to be with oxygenated functional groups of the SWNT. After Fourier transformation, as seen in Fig. 1(b), the peak of the Pt/cSWNT sample is of the same shape but much lower amplitude than that of the Pt foil, which verifies that our Pt/cSWNT catalyst has been almost totally reduced under such conditions, and indicates that the coordination number of Pt atoms in reduced Pt/cSWNT is much less than that in Pt foil. Thus, the Pt species form very small particles after reduction. However, the small shoulder at around 1.4 Å suggests that there may be a small amount of platinum oxide or platinum carbide, or alternatively this shoulder may indicate the close interaction between the Pt nanoparticle and the oxygenated functional groups of the support [21,22]. The fitting result of the EXAFS data gives an average coordination number of 7.80 and the corresponding particle size is 1.16 nm, according to the model by Calvin et al. [23]. The Pt particle size from EXAFS matches very well with the size measured by transmission electron microscope (TEM), as shown in Figure S1 in the supplementary data. Our previous results showed that all Pt nanoparticles prepared from the wet-reduction method give particle sizes of 2–3 nm [4]. Combining Table 1 and the particle size information, it is suggested that smaller Pt particles formed by incipient wetness impregnation lead to lower activity, which is unusual in catalysis. However, de Jong and co-workers have reported similar deactivation phenomenon in carbon nanofiber supported catalysis, and they suggested that the surface oxygen-containing groups, introduced by nitric acid treatment, prevents close contact between reactant and the catalytic particles, leading to low activity [24,25]. Since most of our catalytic particles are also on the outer surface of SWNT, the surface oxygen-containing groups could also be the reason for deactivation in our system. However, we prefer the hypothesis of deactivation by Pt particle chemical interaction with the surface oxygen-containing groups rather than the more physical model of de Jong and co-workers.

3.3. Pt–Co bimetallic catalyst

The reduction of Co in the Pt–Co/cSWNT was followed by taking the time-resolved Co K edge XANES measurements during the hydrogen pre-reduction, and the results are shown in Fig. 2, from which it can be determined that there are three stages during the reduction of Co. The first stage is the decomposition of cobalt nitrate to cobalt oxide, following by the reduction of cobalt oxide, the second stage, with the third stage being the formation of an alloy phase. The change of the existing state of Co can be followed by both the pre-edge XANES feature (the small peak below 7710 eV) and the white line (the most intense peak) change, which can be seen more clearly from the inset of Fig. 2.

The detailed comparison of the Co K edge XAS spectra of Pt–Co/cSWNT before and after hydrogen reduction is shown in Fig. 3. From both the absorption spectra and the Fourier-transformed spectra it can be determined that the cobalt in the catalyst before pre-reduction is highly oxidized. However, the catalyst after reduction shows mainly Co(0) metal, with a small amount of Co–Pt bimetallic bonding, as seen from the higher white line intensity than the Co foil in Fig. 3(a). It has been reported that the formation of Pt–Co alloy can be identified from four different features, labeled A, B, C and D in Fig. 3(a) [7,9]. Compared with the Co foil, features C and D are shifted to lower energies. This shift is due to the expansion of unit cell parameters [9,26], indicating Co is involved in a bimetallic phase, alloying with some element with larger atomic radius, which in this case is Pt. Moreover, features A and B are related to the transitions from 1s orbital to 3d, 4s and 4p hybridized orbitals. Thus, the decrease at feature A and increase at

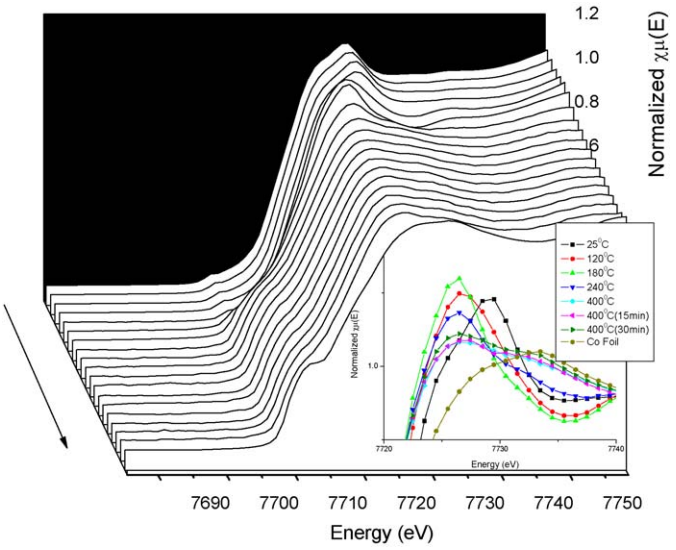

Fig. 2. Time-resolved Co K edge XANES spectra of Pt–Co/cSWNT during hydrogen pre-reduction. The cobalt foil was included as the gray dotted curve. Inset: detailed white lines of selected XANES spectra.

feature B reflects a rearrangement of the hydridization, which strongly depends upon alloying [9].

At the Pt L_{III} edge, Fig. 4(a) shows XANES spectra of Pt–Co/SWNT before and after reduction, in comparison with the Pt foil. Notice that the white line of the catalyst after reduction shifts to the right compared with the Pt foil, indicating that the Pt species in this catalyst is no longer Pt metal, but some alloy species. Also the white line intensity is lower than the Pt foil, indicating the average electron density of the Pt atoms in our catalyst (alloy) is higher than the electron density in Pt foil. A quantitative analysis of the d band vacancies can be achieved by comparing the areas under white line of different samples, and the results are shown in Table 2. The integration area was selected from 10 eV below the edge to 13 eV above the edge according to the literature [27,28]. Thus, the Pt L_{III} edge white line intensity of Pt/cSWNT is a little bit lower than Pt foil, however, the intensity of Pt–Co/cSWNT is much lower. Therefore, it can be concluded that in Pt–Co/cSWNT, Pt is bonding with some element(s) that has a greater electronegativity than hydrogen. This species is probably Co. Combining this with the fact that in Fig. 3(a), the white line intensity of our catalyst at the Co K edge is higher than Co foil, which indicates an electron deficiency, it is very clear that in this catalyst, there is electron transfer from Co to Pt. The R space of the spectra, in Fig. 4(b), shows the bimetallic bonding more clearly, in which the peak position of the reduced catalyst shifts to shorter radial distance by about 0.2 Å, which could be related to the formation of Pt–Co bimetallic bonds.

First shell coordination number fitting was applied to both the Pt L_{III} edge and the Co K edge concurrently, with the following constraints introduced during the fitting [29,30].

$$CN_{Co-Pt} = CN_{Pt-Co} \cdot \frac{x_{Pt}}{x_{Co}},$$

$$R_{Pt-Co} = R_{Co-Pt},$$

$$\sigma^2_{Pt-Co} = \sigma^2_{Co-Pt}$$

Here CN_{Co-Pt} and CN_{Pt-Co} are the average coordination numbers of Pt–Co bonding normalized by total Co amount and total Pt amount, respectively. x_{Pt} and x_{Co} are the atomic compositions, R_{Pt-Co} and R_{Co-Pt} are bond lengths, and σ^2_{Pt-Co} and σ^2_{Co-Pt} are uncertainties of bond lengths after the fitting. The fitting results are listed in Table 3, which shows that from the Pt L_{III} edge data, the average Pt–Co coordination number is very high while the average Pt–Pt coordination number is negligible, indicating that Pt is almost atomically dispersed in Co. For the Co K edge data, on the contrary, both Co–Co and Co–Pt bonds exist. $CN_{Co-Co}/CN_{Co-Pt} = 2.57 < x_{Co}/x_{Pt} = 3.33$ indicates negative tendency of Co clustering, i.e., a Co atom is preferably bonding with a Pt atom rather than another Co atom [29].

To further explore the bimetallic structure, we define:

$$CN_{Co-M} = CN_{Co-Pt} + CN_{Co-Co} = 7.78$$

$$CN_{Pt-M} = CN_{Pt-Pt} + CN_{Pt-Co} = 7.26$$

$$CN_{M-M} = CN_{Pt-M}x_{Pt} + CN_{Co-M}x_{Co} = 7.66$$

CN_{M-M}, the average coordination number of metal–metal bond, is directly related to the average number of atoms per catalytic particle [29]. This number here is close to the average Pt–Pt coordination number in Pt/cSWNT catalyst, indicating they have comparable catalytic particle size in terms of number of atoms per particle. Actually the Pt–Co/cSWNT catalyst has a little smaller average coordination number, i.e., a smaller number of atoms per catalytic particle, however, the lattice parameter should be enlarged due to the addition of Pt, thus these two catalysts should have similar particle size, which is also verified by TEM images, as shown in Figures S1 and S2 in the supplementary data. On the other hand, CN_{Pt-M} is a little smaller than CN_{Co-M}, so Pt has less

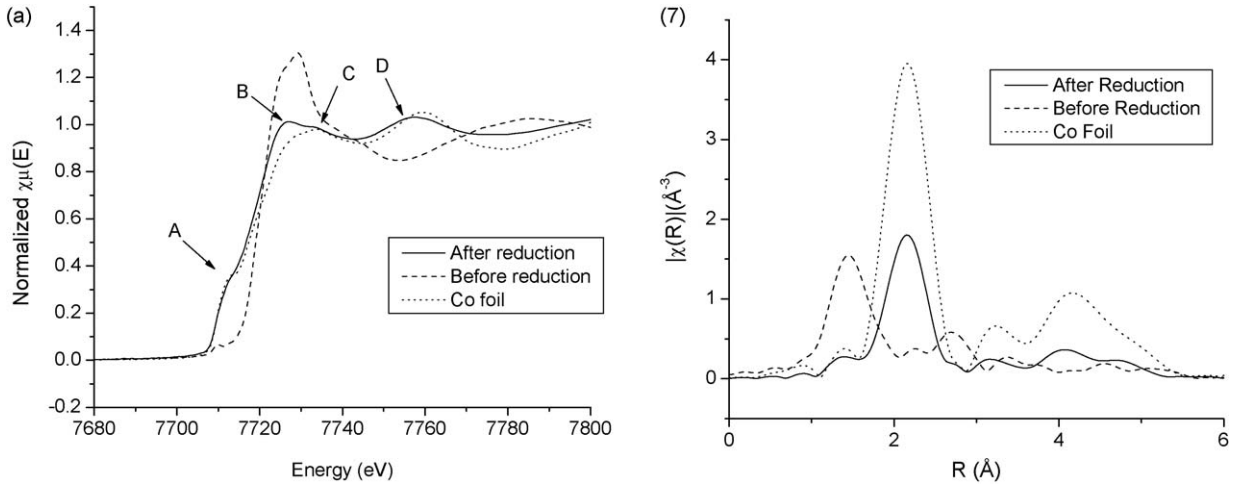

Fig. 3. XAS results at Co edge of Pt–Co/cSWNT before and after reduction. (a) XANES spectra; (b) R space of the EXAFS spectra.

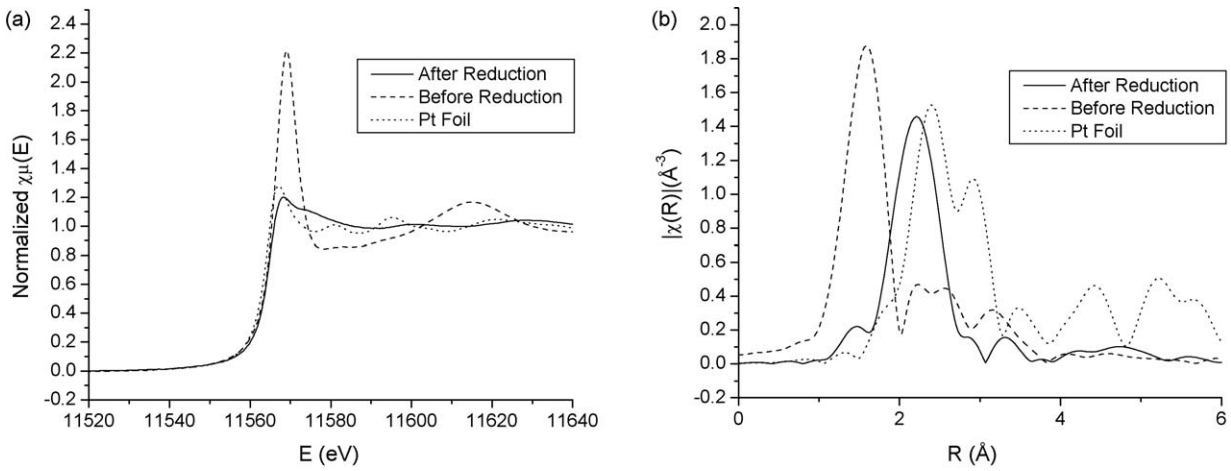

Fig. 4. XAS results at Pt edge of Pt–Co/cSWNT before and after reduction. (a) XANES spectra; (b) R space of the EXAFS spectra.

neighboring atoms than Co, suggesting Pt atoms are more likely to locate at the outer shell of the catalytic particles. In addition, the high activity of the Pt–Co/cSWNT catalyst also suggests that the Pt species are in contact with the aqueous reactants, because Co monometallic catalyst has almost no APR reactivity [4,5]. For bimetallic alloys, Vegard's law suggests the lattice parameter (therefore, bond length) has a linear relationship with the atomic composition [31]. Therefore, from the bond length information in Table 3, it can be calculated that the Co:Pt atomic ratio in the bimetallic alloy phase is about 2:1, which is smaller than the nominal 3.3:1 Co:Pt ratio in the catalyst. From the above analysis, we hypothesize that in this Pt–Co/cSWNT catalyst, the bimetallic nanoparticles have a core–shell structure with Co as the core and Pt–Co alloy phase as the shell.

In order to make better use of noble metals, non-noble-metal-core/noble-metal-shell structure has been developed by depositing a Pt monolayer on the surface of non-noble-metal nanoparticles [32]. However, in our case not only the conversion, but also the selectivity changes when Co is introduced with Pt to form a catalyst. Thus, Co may be in contact with the aqueous reactants, i.e., may not be fully covered by Pt, or more likely, Co affects the reactivity of Pt by electronic pertubation. Davis and co-workers obtained similar submonolayer structures with Pt–Ru bimetallic catalyst, which combined the advantage of Pt and Ru monometallic catalysts [33]. Therefore, in our Pt–Co/cSWNT catalyst, we hypothesize that the increase of activity comes from the higher dispersion of Pt as well as the co-catalytic or modification effect from the Co species. Our previous research showed that the co-existence of individual Pt and Co nanoparticles can greatly increase the conversion of the APR reaction with respect to Pt monometallic catalyst, but alkane selectivity is also increased. In the Pt–Co/cSWNT catalyst here, the selectivity is maintained or even improved, probably due to the close contact of Pt and Co species.

Table 2
The white line area of different catalysts.

Sample	Pt foil	Pt/cSWNT[a]	Pt–Co/cSWNT[a]
Area (eV)	17.05	17.02	16.94
Difference (eV)[b]	–	−0.03	−0.11

[a] Both catalysts are after reduction.
[b] The difference spectra between the catalyst and Pt foil.

Table 3
The EXAFS fitting results for the Pt–Co/cSWNT catalyst.

Absorber	Scatterer	CN[a]	d*R* (Å)[b]	*R* (Å)[c]
Pt	Co	7.26 (0.78)[d]	−0.19 (0.01)[d]	2.58[e]
Co	Pt	2.18[e]	0.08[e]	2.58[e]
	Co	5.60 (0.51)[d]	0.00 (0.00)[d]	2.49[e]

[a] Coordination number of each absorber–scatterer pair.
[b] Deviation from the interatomic distance in pure metal, which is 2.77 Å for Pt and 2.50 Å for Co.
[c] Calculated bond length from d*R*.
[d] Data from the first shell coordination number fitting; data in the brackets are uncertainties given by the IFEFFIT software.
[e] These data are not directly from the fitting thus uncertainty data is not included.

4. Conclusion

By simple sequential impregnation of $Pt(NH_3)_4(NO_3)_2$ and $Co(NO_3)_2$ on SWNT, a Pt–Co bimetallic catalyst is obtained. Compared with the monometallic catalysts, the Pt–Co/SWNT bimetallic catalyst has much higher APR activity but the selectivity is not affected. XAS spectra indicate a core–shell structure with Co as the core and a Pt–Co alloy phase as the shell, where Pt was atomically dispersed. The high APR activity verifies that the Pt species is on the outer surface of the catalytic particles. However, the Co may not be fully covered by Pt, and thus Co may also affect the activity and selectivity as we reported previously [4]. This work demonstrates a new route for the design of bimetallic APR catalysts. Further work is on going to develop Pt based bimetallic APR catalysts with high conversion and good selectivity.

Acknowledgments

The authors are grateful to the DOE, Office of Basic Energy Sciences, grant FG02-05ER15732, for financial support. We acknowledge NSLS at Brookhaven National Laboratory for X-ray beamtime at beamline X18B, and thank Dr. Nebojsa Marinkovic for the on-site technical support. We also acknowledge Prof. Anatoly Frenkel and Dr. Qi Wang at Yeshiva University for their help in EXAFS data analysis. The suggestions and discussions from the reviewers are also greatly appreciated.

Appendix A. Supplementary data

Supplementary data associated with this article can be found, in the online version, at doi:10.1016/j.cattod.2009.02.010.

References

[1] K.V. Kordesch, GR. Simader, Chem. Rev. 95 (1995) 191.
[2] X. Cheng, Z. Shi, N. Glass, L. Zhang, J.J. Zhang, D.T. Song, Z.-S. Liu, H.J. Wang, J. Shen, J. Power Sources 165 (2007) 739.
[3] R.D. Cortright, R.R. Davda, J.A. Dumesic, Nature 418 (2002) 964.
[4] X.M. Wang, N. Li, C. Wang, W.R. Swchartz, S. Lim, T. Fadel, L.D. Pfefferle, G.L. Haller, J. Catal., submitted for publication.
[5] G.W. Huber, J.W. Shabaker, S.T. Evans, J.A. Dumesic, Appl. Catal., B Environ. 62 (2006) 226.
[6] J.W. Shabaker, G.W. Huber, R.R. Davda, R.D. Cortright, J.A. Dumesic, Catal. Lett. 88 (2003) 1.
[7] C. Leroux, M.C. Cadeville, V. Perron-Bohnes, G. Inden, F. Hinz, J. Phys. F: Met. Phys. 18 (1988) 2033.
[8] B.C. Beard, P.N. Ross Jr., J. Electrochem. Soc. 137 (1990) 3368.
[9] E.K. Hlil, R. Baudoing-Savois, B. Moraweck, A.J. Renouprez, J. Phys. Chem. 100 (1996) 3102.
[10] L. Guczi, D. Bazin, I. Kovacs, L. Borko, Z. Schay, J. Lynch, P. parent, C. Lafon, G. Stefler, Zs. Koppany, I. Sajo, Top. Catal. 20 (2002) 129.
[11] G. Jacobs, J.A. Chaney, P.M. Patterson, T.K. Das, J.C. Maillot, B.H. Davis, J. Synchrotron Rad. 11 (2004) 414.
[12] U.A. Paulus, A. Wokaun, G.G. Sherer, T.J. Schmidt, V. Stamenkovic, V. Radmilovic, N.M. Markovic, P.N. Ross, J. Phys. Chem. B 106 (2002) 4181.
[13] H. Yano, J.M. Song, H. Uchida, M. Watanabe, J. Phys. Chem. C 112 (2008) 8372.
[14] J.-I. Park, J. Cheon, J. Am. Chem. Soc. 123 (2001) 5743.
[15] J.-I. Park, M.G. Kim, Y.-W. Jun, J.S. Lee, W.-R. Lee, J. Cheon, J. Am. Chem. Soc. 126 (2004) 9072.
[16] D.C. Koningsberger, R. Prins, X-Ray Absorption: Principles, Applications, Techniques of EXAFS, SEXAFS and XANES, John Wiley & Sons Inc., 1988.
[17] V. Lordi, N. Yao, J. Wei, Chem. Mater. 13 (2001) 733.
[18] M. Newville, J. Synchrotron Rad. 8 (2001) 322.
[19] F.W. Lytle, R.B. Greegor, E.C. Marques, D.R. Sandstrom, G.H. Via, J.H. Sinfelt, J. Catal. 95 (1985) 546.
[20] N.S. Yao, C. Pinckney, S. Lim, C. Pak, G.L. Haller, Microporous Mesoporous Mater. 44–45 (2001) 377.
[21] J. Zhou, X. Zhou, X. Sun, R. Li, M. Murphy, Z. Ding, X. Sun, T.-K. Sham, Chem. Phys. Lett. 437 (2007) 229.
[22] Y. Zhang, M.L. Toebes, A. van der Eerden, W.E. O'Grady, K.P. de Jong, D.C. Koningsberger, J. Phys. Chem. B 108 (2004) 18509.
[23] S. Calvin, M.M. Miller, R. Goswami, S.F. Cheng, S.P. Mulvaney, L.J. Whitman, V.G. Harris, J. Appl. Phys. 94 (2003) 778.
[24] M.L. Toebes, Y.H. Zhang, J. Hajek, T.A. Nijhuis, J.H. Bitter, A.J. van Dillen, D.Y. Murzin, D.C. Koningsberger, K.P. de Jong, J. Catal. 226 (2004) 215.
[25] M.L. Toebes, T.A. Nijhuis, J. Hajek, J.H. Bitter, A.J. van Dillen, D.Y. Murzin, K.P. de Jong, Chem. Eng. Sci. 60 (2005) 5682.
[26] B. Moraweck, A.J. Renouprez, E.K. Hlil, R. Baudoing-Savois, J. Phys. Chem. 97 (1993) 4288.
[27] M. Brown, R.E. Peierls, D.E. Stern, Phys. Rev. B 15 (1977) 738.
[28] K. Sasaki, J.L. Zhang, J. Wang, F. Uribe, R. Adzic, Res. Chem. Intermed. 32 (2006) 543.
[29] A. Frenkel, Z. Kristallogr. 222 (2007) 605.
[30] M.R. Knecht, M.G. Weir, A.I. Frenkel, R.M. Crooks, Chem. Mater. 20 (2008) 1019.
[31] L. Vegard, Z. Phys. 5 (1921) 17.
[32] J. Zhang, F.H.B. Lima, M.H. Shao, K. Sasaki, J.X. Wang, J. Hanson, R.R. Adzic, J. Phys. Chem. B 109 (2005) 22701.
[33] E.P. Maris, W.C. Ketchie, M. Murayama, R.J. Davis, J. Catal. 251 (2007) 281.